Acta Crystallographica Section B
Structural Science
ISSN 0108-7681

Structure and electron density of oxysulfide $Sm_2Ti_2S_2O_{4.9}$, a visible-light-responsive photocatalyst

Masatomo Yashima,[a]* Kiyonori Ogisu[b] and Kazunari Domen[b]

[a]Department of Materials Science and Engineering, Interdisciplinary Graduate School of Science and Engineering, Tokyo Institute of Technology, Nagatsuta-cho 4259, Midori-ku, Yokohama, 226-8502, Japan, and [b]Department of Chemical System Engineering, School of Engineering, The University of Tokyo, 7-3-1 Hongo, Bunkyo-ku, Tokyo, 113-8656, Japan

Correspondence e-mail: yashima@materia.titech.ac.jp

Received 13 January 2008
Accepted 19 March 2008

We report the crystal structure and electron density of samarium titanium oxysulfide, $Sm_2Ti_2S_2O_{4.9}$, photocatalyst obtained through the Rietveld analysis, maximum-entropy method (MEM) and MEM-based pattern fitting of the high-resolution synchrotron powder diffraction data taken at 298.7 K. The $Sm_2Ti_2S_2O_{4.9}$ has a tetragonal structure with the space group *I*4/*mmm*. Refined occupancy factors at the 'equatorial' O1 and 'apical' O2 sites were 0.994 (3) and 0.944 (12), respectively, which strongly suggest oxygen deficiency at the O2 site. Electron-density analyses based on the synchrotron diffraction data of $Sm_2Ti_2S_2O_{4.9}$ in combination with density-functional theory (DFT) calculations of stoichiometric $Sm_2Ti_2S_2O_5$ reveal covalent bonds between Ti and O atoms, while the Sm and S atoms are more ionic. The presence of S 3*p* and O 2*p* orbitals results in increased dispersion of the valence band, raising the top of the valence band and making the material active at visible wavelengths. The present DFT calculations of stoichiometric $Sm_2Ti_2S_2O_5$ indicate the possibility of overall splitting of water, although $Sm_2Ti_2S_2O_{4.9}$ works as a visible-light-responsive photocatalyst in aqueous solutions only in the presence of sacrificial electron donors or acceptors. The oxygen deficiency and cocatalyst seem to be factors affecting the catalytic activity.

1. Introduction

Metal-oxide photocatalysts have been the subject of extensive research for the purposes of solar-energy conversion and environmental remediation (Fujishima & Honda, 1972; Fujishima *et al.*, 2000; Hoffmann *et al.*, 1995; Mills & Le Hunte, 1997; Carp *et al.*, 2004). Overall water splitting using a photocatalyst is an attractive solution for the supply of clean and recyclable hydrogen energy, and there are also a number of photocatalysts that decompose waste materials and hazardous compounds. Although many photocatalysts have been proposed to date, most function only in the ultraviolet ($\lambda <$ 400 nm) region (*e.g.* TiO_2; Fujishima & Honda, 1972; Fujishima *et al.*, 2000) owing to the inherently large band gap of the metal oxides used as a basis for the catalysts. Metal oxysulfides, on the other hand, have the potential to photocatalyze various reactions under visible light. For example, promising results have been reported for $Sm_2Ti_2S_2O_5$, which has been demonstrated to be responsive to excitation at wavelengths up to *ca* 650 nm (Ishikawa *et al.*, 2002, 2003, 2004). The $Sm_2Ti_2S_2O_5$ functions as a stable photocatalyst for the reduction of H^+ to H_2 and oxidation of H_2O to O_2 in the presence of a sacrificial electron donor and acceptor under visible-light irradiation.

The crystal structure of $Sm_2Ti_2S_2O_5$ has been studied by Boyer *et al.* (1999) and Goga *et al.* (1999), revealing a stacking

Table 1
Experimental details.

Crystal data	
Chemical formula	$O_{9.84}S_4Sm_4Ti_4$
M_r	1078.61
Cell setting, space group	Tetragonal, *I*4/*mmm*
Temperature (K)	298.7
a, *c* (Å)	3.82123 (2), 22.96371 (12)
V (Å^3)	335.31 (1)
Z	1
D_x (Mg m^{-3})	5.342
Radiation type	Synchrotron
Specimen form, colour	Circular flat plate, yellow to yellowish-green
Specimen size	20 mm diam., 0.5 mm height
Specimen preparation cooling rate (K min^{-1})	10
Specimen preparation pressure (kPa)	100
Specimen preparation temperature (K)	1173
Data collection	
Diffractometer	A multiple-detector system with Ge(111) analyzer crystals, Soller slits and scintillation counters (Toraya *et al.*, 1996)
Data collection method	Specimen mounting: flat specimen; mode: reflection; scan method: step
2θ (°)	$2\theta_{min}$ = 7.05050, $2\theta_{max}$ = 154.887, increment = 0.01
Refinement	
Refinement method	Rietveld
R factors and goodness-of-fit	R_p = 0.0535, R_{wp} = 0.0689, *S* = 1.56
Wavelength of incident radiation (Å)	1.20643
Excluded region(s)	None
Profile function	Split Pearson (Toraya, 1990)
No. of reflections	274
No. of parameters	10

Computer programs: *Rigaku software* (Toraya *et al.*, 1996), *RIETAN*-2000 (Izumi & Ikeda, 2000), *VESTA* (Momma & Izumi, 2006).

structure in which Sm_2S_2 slabs of a rock-salt type (layers of two-atom thickness) are stacked in the *c*-axis direction and were separated by a two-dimensional network of corner-sharing octahedra [= Ti_2O_5] having an ReO_3 structure. Ishikawa *et al.* (2002, 2003, 2004) discussed the photocatalytic activity of $Sm_2Ti_2S_2O_5$ based on UV–vis spectroscopy, X-ray photoemission spectroscopy and electrochemical analysis, and its electronic band structure analysis on the basis of DFT calculations. However, the electron-density distribution of $Sm_2Ti_2S_2O_5$, useful information in the investigation of chemical bonding and a key basis for understanding photocatalytic activity (Yashima, Lee & Domen, 2007), has yet to be reported.

In the present work, the crystal structure and electron-density distribution of an $Sm_2Ti_2S_2O_{4.9}$ photocatalyst under visible-light excitation are investigated by synchrotron powder diffraction. Here the $Sm_2Ti_2S_2O_{4.9}$ sample is the same as $Sm_2Ti_2S_2O_5$ in the literature (Ishikawa *et al.*, 2004). In the present work we show the oxygen deficiency (δ) in $Sm_2Ti_2S_2O_{5-\delta}$: $Sm_2Ti_2S_2O_{4.9}$. The electron density of $Sm_2Ti_2S_2O_5$ was also studied by the DFT calculations where we analyzed an approximate stoichiometric $Sm_2Ti_2S_2O_5$ composition for ease of calculation.

2. Experiments and data analysis

2.1. Sample preparation

Samarium titanate ($Sm_2Ti_2O_7$) was prepared by the Pechini method using $Ti(O^iPr)_4$ and $Sm(NO_3)\cdot 6H_2O$ as starting materials according to the literature method (Ishikawa *et al.*, 2004; Pechini, 1967). The resultant $Sm_2Ti_2O_7$ powder was heated under flowing H_2S (flow rate: 10 ml min^{-1}) at 1173 K for 1 h to yield a yellow to yellowish-green powder. This powder functioned as a stable and efficient photocatalyst for the splitting of water into H_2 and O_2 in the presence of a sacrificial electron donor (0.01 *M* Na_2S and 0.01 *M* Na_2SO_3) or acceptor (0.01 *M* $AgNO_3$; Ishikawa *et al.*, 2002). The chemical composition of the $Sm_2Ti_2S_2O_{4.9}$ sample was determined by inductively coupled plasma optical emission spectroscopy (ICP-OES) using a Horiba instrument combined with a Horiba sulfur–carbon determinator and an LECO oxygen–nitrogen determinator. The molar Sm:Ti:S:O ratio of the prepared samples was determined to be 2.00 (2):2.01 (1):2.11 (1):4.92 (1), indicating oxygen deficiency with a chemical formula of $Sm_2Ti_2S_2O_{4.9}$ (values in parentheses denote error in the last digit). The oxygen deficiency is consistent with the existence of a small amount of Ti^{3+} species, as reported in the literature (Ishikawa *et al.*, 2003). The excess sulfur is attributable to the residual sulfur at the surface of the powder, formed during sulfurization by H_2S in the sample preparation.

2.2. Synchrotron powder diffraction experiment and data processing

Table 1 gives a summary of the experimental details.[1] Synchrotron X-ray powder diffraction analyses were performed using the multiple-detector system (Toraya *et al.*, 1996) installed at the BL-4B$_2$ beamline of the Photon Factory operated by the High Energy Accelerator Research Organization (KEK), Japan. The experimental setup consisted of a bending-magnet light source, a double-crystal Si(111) monochromator, a focusing cylindrical mirror and a multiple-detector system with Ge(111) analyzer crystals, Soller slits and scintillation counters (Toraya *et al.*, 1996). A monochromated 1.20643 Å X-ray beam was utilized. Powder diffraction data from the sample at 298.7 K in air were collected in asymmetric flat-specimen reflection geometry with a fixed incident angle of 7.0°. Scanning parameters were set as follows: step interval 0.01°; counting time 9.5 s per step; diffraction angle (2θ) 8–155°. The crystal structure of the $Sm_2Ti_2S_2O_{4.9}$ sample was refined by the Rietveld method using *RIETAN*-2000 (Izumi & Ikeda, 2000). As enhancement in the asymmetric scan mode is not implemented in *RIETAN*-2000, the observed intensity data were modified by multiplying the term $\{1 + [\sin\alpha/\sin(2\theta - \alpha)]\}/2$, where α is the fixed incident angle, in order to obtain data equivalent to those measured in the symmetric scan mode (Toraya *et al.*, 1993). The peak shape

[1] Supplementary data for this paper are available from the IUCr electronic archives (Reference: OG5028). Services for accessing these data are described at the back of the journal.

Table 2
Refined crystallographic parameters for $Sm_2Ti_2S_2O_{4.9}$ and reliability factors for synchrotron powder diffraction data (298.7 K).

Atom/site	Wyckoff position	Occupancy g	Atomic coordinates x	y	z	Atomic displacement parameters U (Å^2)
Sm	4(*e*)	1.0	0.0	0.0	0.33382 (1)	0.00320 (12)
Ti	4(*e*)	1.0	0.0	0.0	0.07819 (4)	0.0039 (2)
S	4(*e*)	1.0	0.0	0.0	0.20364 (7)	0.0046 (2)
O1	8(*g*)	0.994 (3)	0.0	1/2	0.09734 (9)	0.0067 (6)
O2	2(*a*)	0.944 (12)†	0.0	0.0	0.0	0.0093 (13)

Unit cell: tetragonal *I*4/*mmm*, $a = b = 3.82123$ (2), $c = 22.96371$ (12) Å, $\alpha = \beta = \gamma = 90°$, $V = 335.312$ (3) Å^3. † Linear constraint for the occupancy factors at O1 and O2 sites: $g(O2) = 4.92 - 4 \times g(O1)$. Reliability factors in Rietveld analysis: $R_{wp} = 0.0689$, GOF = 1.56, $R_I = 0.0107$, $R_F = 0.0060$. Reliability factors in first MEM analysis: $R_F = 0.0057$, $wR_F = 0.0056$. Reliability factors in first MPF analysis: $R_{wp} = 0.0687$, GOF = 1.56, $R_I = 0.0080$, $R_F = 0.0049$. Wavelength = 1.20643 Å.

was assumed to be a split Pearson VII-type function (Toraya, 1990), and the cut-off value was set at 30.00 times the full width at half-maximum (FWHM). Background intensities were fit using a Legendre polynomial function with 12 parameters. The 12 variables were refined simultaneously with the unit-cell, zero-point, scale, profile-shape and crystal structural parameters. The preferred orientation of the $Sm_2Ti_2S_2O_{4.9}$ sample along the [001] direction was corrected by the March–Dollase function. The electron-density distribution of $Sm_2Ti_2S_2O_{4.9}$ was investigated by the maximum-entropy method (MEM) using the 249 structure factors obtained by the Rietveld analysis. MEM calculations were carried out using the computer program *PRIMA* (Izumi & Dilanian, 2002) with a $32 \times 32 \times 192$ pixel unit cell. To confirm the validity of the MEM analysis, MEM-based pattern fitting (MPF; Izumi & Dilanian, 2002) was also conducted using the structure factors obtained by Fourier transform of the MEM electron-density distribution. It is well known that the MEM can produce an accurate electron-density distribution that visualizes covalent bonding (Yashima & Tanaka, 2004; Yashima & Tsunekawa, 2006; Yashima *et al.*, 2006; Yashima, Lee & Domen, 2007; Yashima, Ando & Tabira, 2007).

2.3. DFT calculation

The *Vienna Ab Initio Simulation Package* (*VASP*; Kresse & Hafner, 1993; Kresse & Furthmuller, 1996) was employed to calculate the valence electron-density distribution and partial density of states in stoichiometric $Sm_2Ti_2S_2O_5$ and $Sm_2Ti_2O_7$. Calculations were performed using projector-augmented wave (PAW) potentials for Sm, Ti, S and O atoms (Kresse & Joubert, 1999; Blöchl, 1994), and a plane-wave basis set with a cutoff of 500 eV. The Perdew–Burke–Ernzerhof (PBE) generalized gradient approximation (GGA) was employed for the exchange and correlation functional (Perdew *et al.*, 1996). Sums over occupied electronic states of $Sm_2Ti_2S_2O_5$ were performed using the Monkhorst–Pack scheme (Monkhorst & Pack, 1976) on a $5 \times 5 \times 1$ set of the *k*-point mesh. The unit-cell and positional parameters refined using the synchrotron data for $Sm_2Ti_2S_2O_{4.9}$ were used for comparison with the experimental results without structural optimization in *VASP* calculations of stoichiometric $Sm_2Ti_2S_2O_5$. DFT calculations of $Sm_2Ti_2O_7$ were also conducted using the unit-cell and positional data reported in the literature (MacLean *et al.*, 1979). Sums over occupied electronic states were performed using the Monkhorst–Pack scheme (Monkhorst & Pack, 1976) on a $5 \times 5 \times 5$ set of the *k*-point mesh.

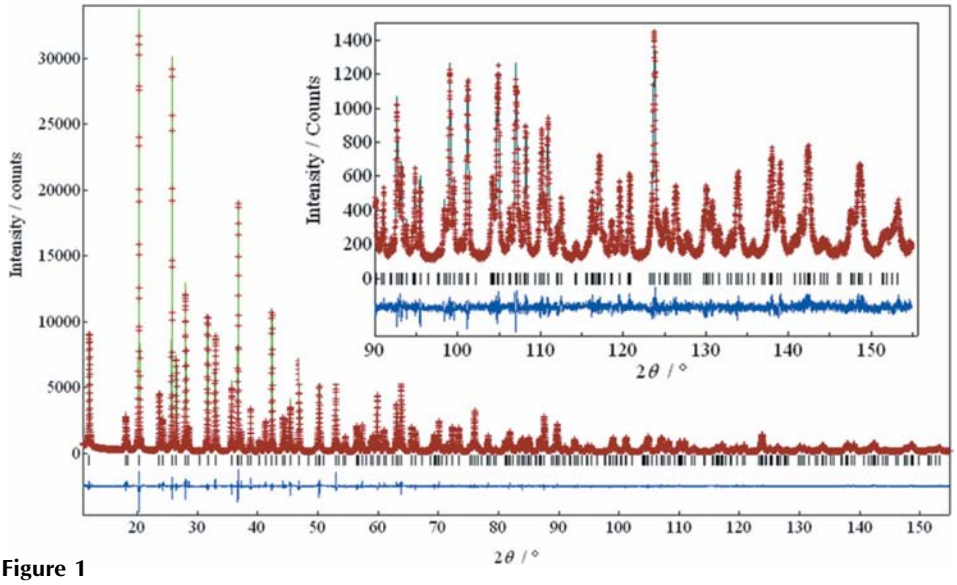

Figure 1
Whole powder pattern determined by the first MPF analysis of the synchrotron powder diffraction data of $Sm_2Ti_2S_2O_{4.9}$ at 299 K. (Inset) Enlargement of pattern. Plots (red crosses) denote observed data, green lines denote calculated profiles and blue lines denote the difference. Vertical black lines indicate the positions of possible Bragg peaks of the tetragonal *I*4/*mmm* $Sm_2Ti_2S_2O_{4.9}$ phase. This figure is in colour in the electronic version of this paper.

3. Results and discussion

3.1. Rietveld refinement and crystal structure of $Sm_2Ti_2S_2O_{4.9}$

All reflections in the synchrotron powder diffraction profile (Fig. 1) were indexed as belonging to a tetragonal cell, indicating a single phase of Ruddlesden–Popper-type $Sm_2Ti_2S_2O_{4.9}$. Rietveld analyses of the synchrotron diffraction data were thus performed assuming a Ruddlesden–Popper-type structure (Boyer *et al.*, 1999; Goga *et al.*, 1999). In a preliminary analysis of the synchrotron powder diffraction data, refinement gave an occupancy factor at the S site g(S) of 0.998 (5), which is consistent with the chemical analysis. The occupancy factor g(S) was there-

fore fixed at unity in the final refinement. Isotropic atomic displacement parameters were assumed for all the atoms. A preliminary analysis of the occupancy factors of O sites suggested a small degree of oxygen deficiency, which is reasonably consistent with the results of chemical analyses. The occupancy factors at the O1 and O2 sites were refined with a linear constraint, $g(\mathrm{O2}) = 4.92–4g(\mathrm{O1})$, where the value of 4.92 was obtained in the chemical analyses. The calculated intensity obtained after final refinement is in good agreement with the observed data (Fig. 1). The refined crystallographic parameters and reliability factors obtained using synchrotron powder diffraction data (Table 2) are closely consistent with the values reported in the literature (Goga *et al.*, 1999), and have a higher degree of precision (Boyer *et al.*, 1999; Goga *et al.*, 1999).

Figs. 2(*a*) and 3(*a*) show the crystal structure of $Sm_2Ti_2S_2O_{4.9}$ drawn with the refined crystallographic parameters and $TiSO_5$ octahedra. Fig. 4(*a*) shows the crystal structure of $Sm_2Ti_2S_2O_{4.9}$ consisting of atomic layers. The synchrotron diffraction data indicate that the $Sm_2Ti_2S_2O_{4.9}$ material has a Ruddlesden–Popper-type structure (space group *I*4/*mmm*) with refined unit-cell parameters of $a = b = 3.82123$ (2), $c = 22.96371$ (12) Å, $\alpha = \beta = \gamma = 90°$, and $V = 335.312$ (3) Å^3 (299 K). This material has a stacking structure in which Sm_2S_2 slabs of a rock-salt type (layers of two-atom thickness) are stacked in the *c*-axis direction separated by a two-dimensional network of corner-sharing octahedra (= Ti_2O_5) having a ReO_3 structure (Figs. 2*a*, 3*a* and 4*a*). The coordination numbers of Sm, Ti, S, O1 and O2 atoms are 8 (four S and four O1 atoms), 6 (four O1, one O2 and one S atoms), 5 (four Sm and one Ti atoms), 4 (two Sm and two Ti atoms) and 2 (two Ti atoms), respectively. In $Sm_2Ti_2S_2O_{4.9}$ the Ti atom is in an approximately octahedral coordination with four 'equatorial' O atoms (O1) at 1.9606 (5) Å, one 'apical' O atom (O2) at 1.7955 (9) Å, and one S atom at the opposite apex 2.881 (2) Å distant (Fig. 2*a*). The Ti—S distance is a long-bonding distance in $Sm_2Ti_2S_2O_{4.9}$ and Ti lies toward the apical O2 atom, as shown in Figs. 2(*a*) and 3(*a*). These features are consistent with literature reports (Boyer *et al.*, 1999; Goga *et al.*, 1999; Hyett *et al.*, 2004). The bond-valence sums (BVSs) of the Sm, Ti, S, O1 and O2 atoms are estimated to be 3.2, 3.9, 2.0, 2.03 and 1.99, which are consistent with the valences of Sm^{3+}, Ti^{4+}, S^{2-}, O^{2-} and O^{2-} ions, respectively. Bond-valence parameters of 2.55, 2.24, 2.088 and 1.815 are assumed here for Sm—S, Ti—S, Sm—O and Ti—O bonds, respectively (Brese & O'Keeffe, 1991). The valence of the sulfur species (2−) is consistent with the X-ray photoelectron spectroscopy results (Ishikawa *et al.*, 2003). A lower BVS value (1.99) for the O2 site than that (2.03) at the O1 position is consistent with the oxygen deficiency at the O2 site (Table 1).

3.2. Electron density and chemical bonding of $Sm_2Ti_2S_2O_{4.9}$

Figs. 2(*a*) and 3(*a*) show the crystal structure of $Sm_2Ti_2S_2O_{4.9}$ drawn with the refined crystallographic para-

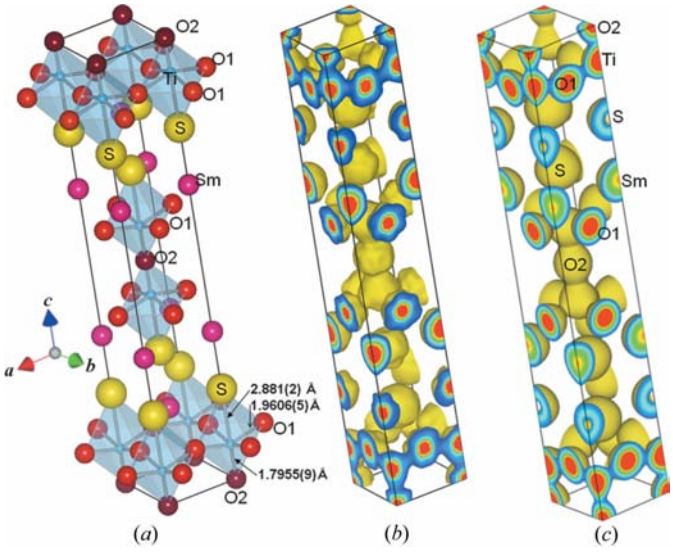

Figure 2
(*a*) Refined crystal structure and (*b*) isosurface of electron density at 0.5 Å^{-3} obtained by MPF analysis of synchrotron powder diffraction data for $Sm_2Ti_2S_2O_{4.9}$. (*c*) Isosurface of valence electron density at 0.5 Å^{-3} obtained by DFT calculations of stoichiometric $Sm_2Ti_2S_2O_5$. Pink, blue, red, dark red and yellow spheres in (*a*) denote Sm, Ti, O1, O2 and S atoms, respectively. $TiSO_{4.9}$ octahedra are shown in (*a*).

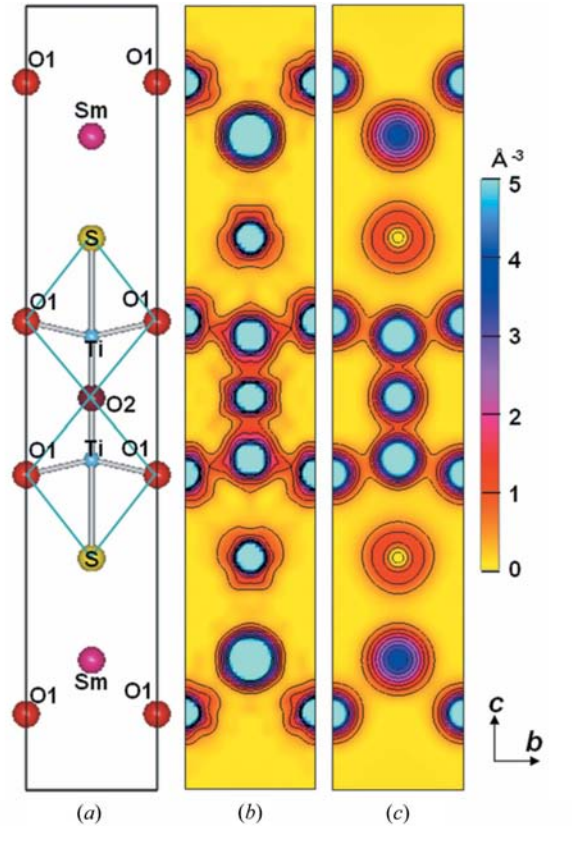

Figure 3
(*a*) Refined crystal structure and (*b*) MEM electron-density distribution on the *bc* plane of $Sm_2Ti_2S_2O_{4.9}$ at $x = \frac{1}{2}$. (*c*) DFT valence electron-density distribution on the *bc* plane of $Sm_2Ti_2S_2O_5$ at $x = \frac{1}{2}$. Black contour lines: 0.5–5 Å^{-3} in 0.5 Å^{-3} steps. Pink, blue, red, dark red and yellow spheres in (*a*) denote Sm, Ti, O1, O2 and S atoms, respectively. $TiSO_{4.9}$ octahedra are shown by the blue solid lines in (*a*).

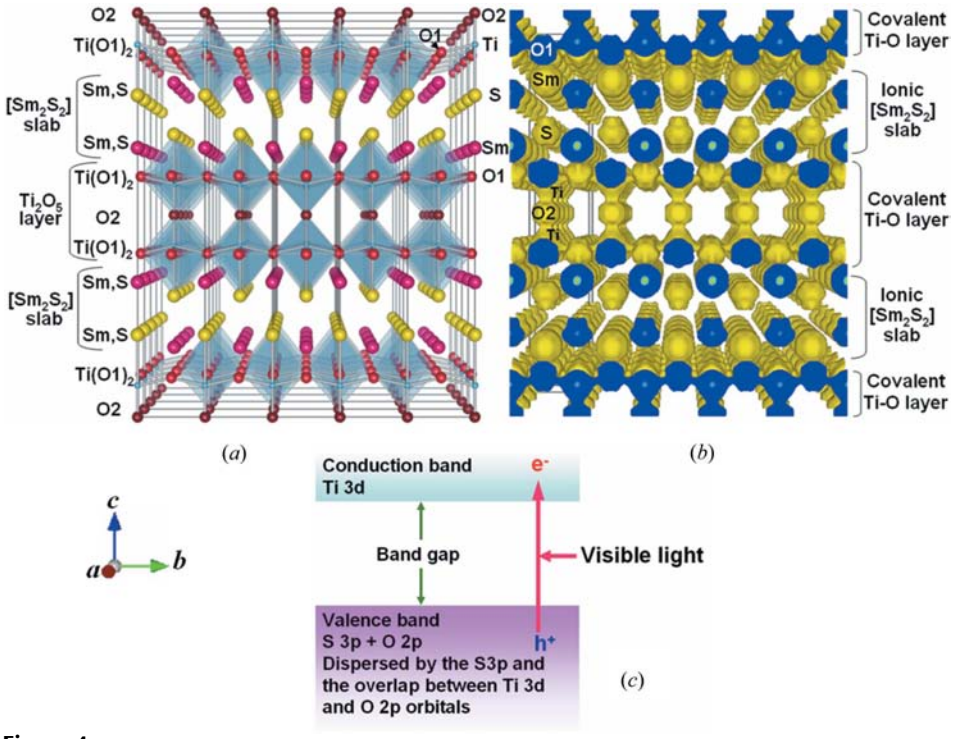

Figure 4
(*a*) Refined crystal structure and (*b*) equi-density surface of MEM electron density at 0.8 Å^{-3} for $Sm_2Ti_2S_2O_{4.9}$. (*c*) Schematic diagram of valence and conduction bands for stoichiometric $Sm_2Ti_2S_2O_5$. Cells of 4 × 5 × 1 are depicted to show the chemical bonding in the crystal structure. Thin solid lines in (*a*) are the unit cells. Pink, blue, red, dark red and yellow spheres in (*a*) denote Sm, Ti, O1, O2 and S atoms, respectively. $TiSO_{4.9}$ octahedra are shown in (*a*). This figure is in colour in the electronic version of this paper.

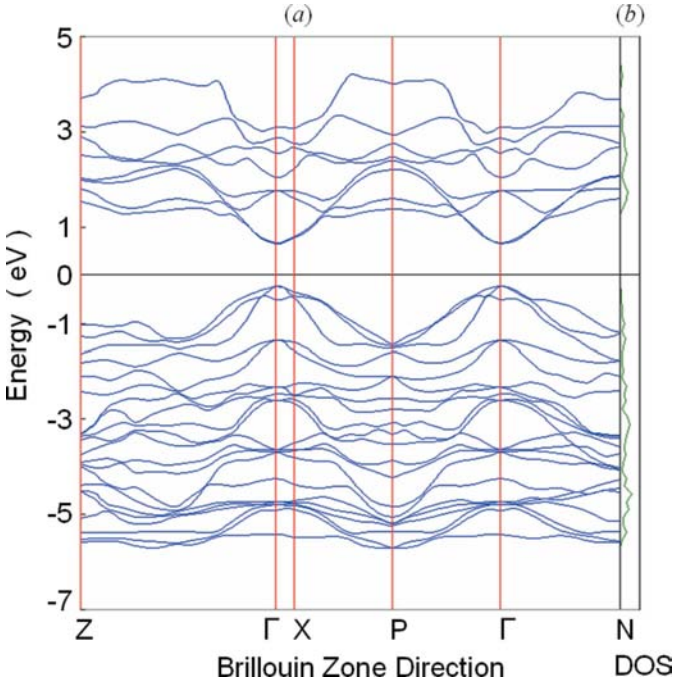

Figure 5
(*a*) Band dispersion and (*b*) corresponding total DOS for $Sm_2Ti_2S_2O_5$.

meters. Fig. 2(*b*) shows the isosurface of electron density for the $Sm_2Ti_2S_2O_{4.9}$ photocatalyst at 0.5 Å^{-3}, as determined by MPF analysis of synchrotron powder diffraction data, and Fig. 2(*c*) shows the corresponding isosurface of valence electron density of stoichiometric $Sm_2Ti_2S_2O_5$ at 0.5 Å^{-3} obtained by DFT calculations. Fig. 3(*b*) shows the MEM electron-density distribution on the *bc* plane of $Sm_2Ti_2S_2O_{4.9}$ at $x = \frac{1}{2}$. Fig. 3(*c*) shows the corresponding DFT valence electron-density distribution of stoichiometric $Sm_2Ti_2S_2O_5$. Fig. 4(*a*) shows the crystal structure of $Sm_2Ti_2S_2O_{4.9}$ consisting of O2, $Ti(O1)_2$, SmS, SmS, $Ti(O1)_2$, O2, $Ti(O1)_2$, SmS, SmS, $Ti(O1)_2$ and O2 layers. Fig. 4(*b*) shows the isosurface of electron density of $Sm_2Ti_2S_2O_{4.9}$ at 0.8 Å^{-3}. The electron-density distribution obtained using synchrotron data of $Sm_2Ti_2S_2O_{4.9}$ (Figs. 2*b* and 3*b*) is consistent with the valence electron-density distribution determined by DFT calculations for stoichiometric $Sm_2Ti_2S_2O_5$ (Figs. 2*c* and 3*c*).

Both maps of MEM electron density for $Sm_2Ti_2S_2O_{4.9}$ and of DFT valence electron density for stoichiometric $Sm_2Ti_2S_2O_5$ clearly indicate covalent bonding between the Ti and O atoms, indicating a two-dimensional network consisting of covalent bonds between Ti and O atoms (Figs. 2*b*, 2*c*, 3*b*, 3*c* and 4*b*). The two-dimensional networks of Ti—O1 covalent bonds exist at z = 0.078–0.098, 0.403–0.422, 0.578–0.597 and 0.903–0.922. The two-dimensional network of Ti—O1 covalent bonds at z = 0.078–0.098 is connected with that at z = 0.903–0.922 through the Ti—O2—Ti covalent bonding at $x = y = \frac{1}{2}$, and the two-dimensional network of Ti—O1 covalent bonds at z = 0.403–0.422 is connected with that at z = 0.578–0.597 through the Ti—O2—Ti covalent bonding at $x = y$ = 0.0.

To investigate the chemical bonding in $Sm_2Ti_2S_2O_{4.9}$, the minimum MEM electron and DFT valence electron densities between atoms were determined. The minimum MEM electron density (MMED) at the Ti—O1 bond (1.0 Å^{-3}) is a little higher than the minimum valence electron density (MVED) at the same bond (0.7 Å^{-3}), while the MMED at the Ti—O2 bond (1.0 Å^{-3}) agrees well with the MVED of the same bond (1.0 Å^{-3}). These minimum electron-density values for the Ti—O bonds (0.7–1.0 Å^{-3}) are higher than for the Ti—S, Sm—S and Sm—O1 bonds (0.2–0.3 Å^{-3}), indicating that the Ti—S, Sm—S and Sm—O1 bonds are more ionic than the Ti—O bonds. The ionic Sm and S atoms form Sm_2S_2 slabs in the crystal structure (Figs. 2*b*, 2*c*, 3*b*, 3*c* and 4*b*). These results

indicate that the chemical bonding in $Sm_2Ti_2S_2O_{4.9}$ forms a stacking structure, which consists of covalent Ti—O layers and ionic Sm_2S_2 slabs (Fig. 4*b*).

Fig. 5 shows the electronic structure of stoichiometric $Sm_2Ti_2S_2O_5$, which was obtained by the DFT calculations. This figure indicates the direct electronic transition at the Γ point. According to the UV–vis diffuse reflectance spectra of $Sm_2Ti_2S_2O_{5-\delta}$ reported in the literature (Ishikawa *et al.*, 2002, 2003, 2004), the absorption edge was not steep against the wavelength, suggesting the indirect electronic transition. Here the δ is the concentration of the oxygen deficiency. The indirect transition can be ascribed to the oxygen deficiency indicated in the synchrotron diffraction and chemical analyses. Fig. 6 shows parts of the total density of states (DOS) and partial DOS diagrams for Sm, S, O1, O2 and Ti. Refer to Fig. 4(*c*) for a schematic diagram of valence and conduction bands of $Sm_2Ti_2S_2O_5$. Covalent bonding between the Ti and O atoms can be attributed to the overlap of Ti 3*d* and O 2*p* orbitals. The top of the valence band is mainly composed of S 3*p* and O 2*p* orbitals, whereas the bottom of the conduction band is composed of Ti 3*d* orbitals, consistent with previous reports (Ishikawa *et al.*, 2002, 2004). A large dispersion of the valence band (*ca* 6 eV) by the presence of the S 3*p* orbital and overlap of the O 2*p* orbital with Ti 3*d* orbitals can be seen in $Sm_2Ti_2S_2O_5$. The visible-light response of $Sm_2Ti_2S_2O_{4.9}$ is thus attributable to the larger dispersion of the valence band, which raises the top of the valence band. These results suggest that the small energy gap exhibited by $Sm_2Ti_2S_2O_{4.9}$ can be primarily attributed to the effect of the S 3*p* and Ti 3*d* states and Ti—O bonds.

The present work has demonstrated covalent bonding at the Ti—O bonds based on electron-density analysis of $Sm_2Ti_2S_2O_{4.9}$ using synchrotron diffraction data combined with DFT calculations of stoichiometric $Sm_2Ti_2S_2O_5$. The DFT calculations also reveal both the presence of S 3*p* orbitals and overlap of the O 2*p* and Ti 3*d* orbitals, resulting in widening of the valence band and thus lower band-gap energy. The band-gap energy determined by the present DFT calculations (0.9 eV) is smaller than that indicated by UV–vis reflectance spectra (1.9–2.3 eV; Ishikawa *et al.*, 2002). This underestimation is reasonable in the local density approximation. The small band-gap energy of $Sm_2Ti_2S_2O_5$ allows the material to be activated as a photocatalyst by the absorption of visible light at wavelengths as long as 650 nm. It is considered that the S 3*p* and Ti 3*d* orbitals and Ti—O covalent bonds are critical to the visible-light photocatalytic activity of $Sm_2Ti_2S_2O_{4.9}$.

$Sm_2Ti_2S_2O_{4.9}$ photocatalyst evolves H_2 or O_2 from aqueous solutions under visible-light irradiation only in the presence of a sacrificial electron donor or acceptor (Ishikawa *et al.*, 2002, 2004), while the present DFT calculations of $Sm_2Ti_2S_2O_5$ confirmed the possibility of a visible-light response for overall water splitting. The present structural analysis has indicated the presence of oxygen deficiency at the O2 site (Table 2), which is a possible factor affecting the catalytic activity. Another possible factor is the cocatalyst, which plays essential roles of inducing the generation of carriers, constructing catalytic gas evolution sites and reducing the activation energy required for gas evolution.

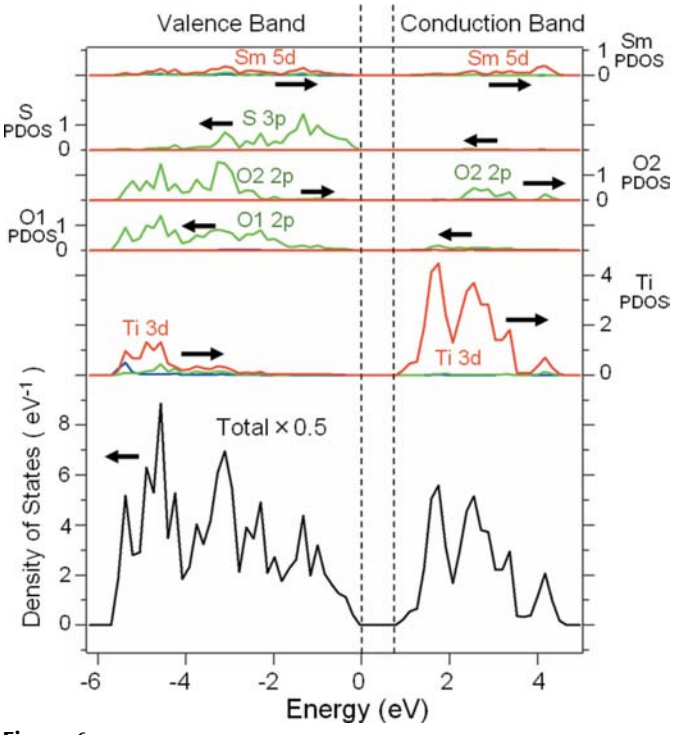

Figure 6
Part of the diagram of total and partial DOS for Ti, O1, O2, S and Sm orbitals in $Sm_2Ti_2S_2O_5$. Blue, green and red lines denote the partial DOS for *s*, *p* and *d* orbitals, respectively. The intensity of blue lines is negligible. The arrow denotes the scale for the DOS. This figure is in colour in the electronic version of this paper.

3.3. Comparison of $Sm_2Ti_2S_2O_{4.9}$ with $Sm_2Ti_2O_7$

It is interesting to compare the chemical bonding and electronic structure of $Sm_2Ti_2S_2O_{4.9}$ with those of $Sm_2Ti_2O_7$, which has a similar chemical formula but a larger band gap

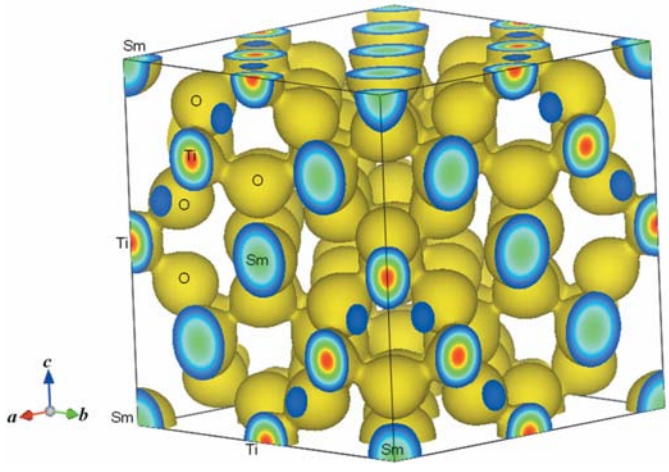

Figure 7
Isosurface of valence electron density at 0.5 Å^{-3} obtained by DFT calculations for pyrochlore-type $Sm_2Ti_2O_7$.

(2.8–3 eV; Ishikawa *et al.*, 2002; Uno *et al.*, 2005). Figs. 7–9 show the isosurfaces of valence electron density at 0.5 Å^{-3}, and the valence electron-density distribution and density of states of the pyrochlore-type $Sm_2Ti_2O_7$, as obtained by DFT calculations. These results clearly indicate covalent bonding between Ti and O atoms, attributed to the overlap of Ti 3*d* and O 2*p* orbitals, whereas the bonding between Sm and O atoms is more ionic. The top of the valence band is mainly composed of O 2*p* orbitals, whereas the bottom of the conduction band is composed of Ti 3*d* orbitals. The width of the valence band of $Sm_2Ti_2O_7$ (*ca* 4.5 eV) is smaller than that of $Sm_2Ti_2S_2O_5$ (*ca* 6 eV), leading to the larger band gap of $Sm_2Ti_2O_7$ (*ca* 3 eV) compared with $Sm_2Ti_2S_2O_5$ (*ca* 1.0 eV). In $Sm_2Ti_2S_2O_5$ the presence of S atoms increases the valence band width, leading to a visible-light response as a photocatalyst. Distortion of the Ti(O_5S) octahedron due to the long bond distance between the S and Ti atoms might also contribute to the visible-light response by raising the top of the O 2*p* valence band.

4. Conclusions

Samarium titanium oxysulfide ($Sm_2Ti_2S_2O_{5-\delta}$), a promising visible-light responsive photocatalyst, was investigated by synchrotron powder diffraction of $Sm_2Ti_2S_2O_{4.9}$ and DFT calculations of stoichiometric $Sm_2Ti_2S_2O_5$. The BVSs for the Sm(S_4O1_4), Ti((O1)$_4$(O2)S), S(Sm_4Ti), O1(Sm_2Ti_2) and O2(Ti_2) coordinations were estimated to be 3.2, 3.9, 2.0, 2.03 and 1.99, consistent with the valences of Sm^{3+}, Ti^{4+}, S^{2-}, O^{2-} and O^{2-} ions, respectively. A lower BVS value (1.99) at the O2 site is consistent with oxygen deficiency at this position. Electron-density analysis based on synchrotron diffraction data of $Sm_2Ti_2S_2O_{4.9}$ in combination with DFT calculations of $Sm_2Ti_2S_2O_5$ clearly showed covalent bonding between Ti and O atoms, and ionic bonding at the Sm—S, Sm—O and Ti—S bonds. The results demonstrate that chemical bonding in $Sm_2Ti_2S_2O_{4.9}$ forms a stacking structure consisting of a two-dimensional network of Ti—O covalent bonds and of ionic Sm_2S_2 slabs (Fig. 4*b*). The overlap of O 2*p* and Ti 3*d* orbitals is responsible for the covalent bonds between Ti and O atoms. The presence of S 3*p* orbitals and overlap of the O 2*p* and Ti 3*d* states result in the enhanced dispersion of the valence band, raising the top of the valence band and realising the visible-light response. The S 3*p* and Ti 3*d* orbitals, and covalent Ti—O bonds are thus expected to be responsible for the small band-gap energy exhibited by $Sm_2Ti_2S_2O_{4.9}$, allowing photocatalysis to occur at visible wavelengths of as long as 650 nm. The S 3*p* and Ti 3*d* orbitals, and covalent Ti—O bonds may thus be a fundamental basis for the design of Ti-based oxysulfide photocatalysts with activity under visible light. The present DFT calculations of stoichiometric $Sm_2Ti_2S_2O_5$ indicate the possibility of overall splitting of water, although $Sm_2Ti_2S_2O_{4.9}$ works as a visible-light photocatalyst in aqueous solutions only in the presence of a sacrificial electron donor or acceptor. The oxygen deficiency and cocatalyst seem to be factors affecting the catalytic activity.

This research was carried out under the user program no. 2008G080 and 2006G264 of Photon Factory. This research was supported in part by the Ministry of Education, Culture, Sport, Science and Technology of Japan through a Grant-in-Aid for Scientific Research (B). The authors express special thanks to Mr T. Komatsu for experimental assistance. Figs. 2, 3, 4, 7 and

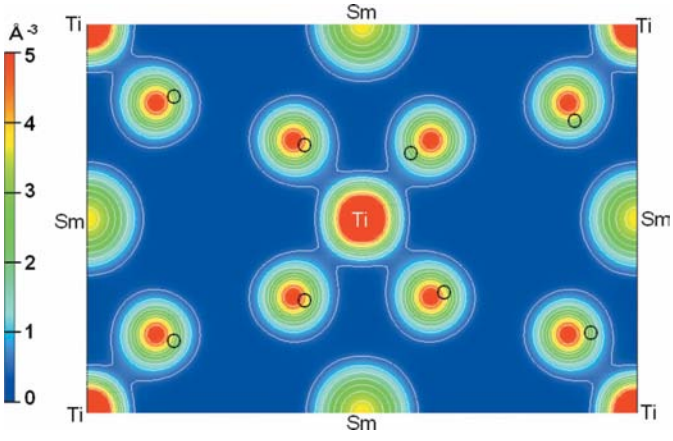

Figure 8
DFT valence electron density distribution on the (110) plane of $Sm_2Ti_2O_7$. White contour lines: 0.5–5 Å^{-3} in 0.5 Å^{-3} steps.

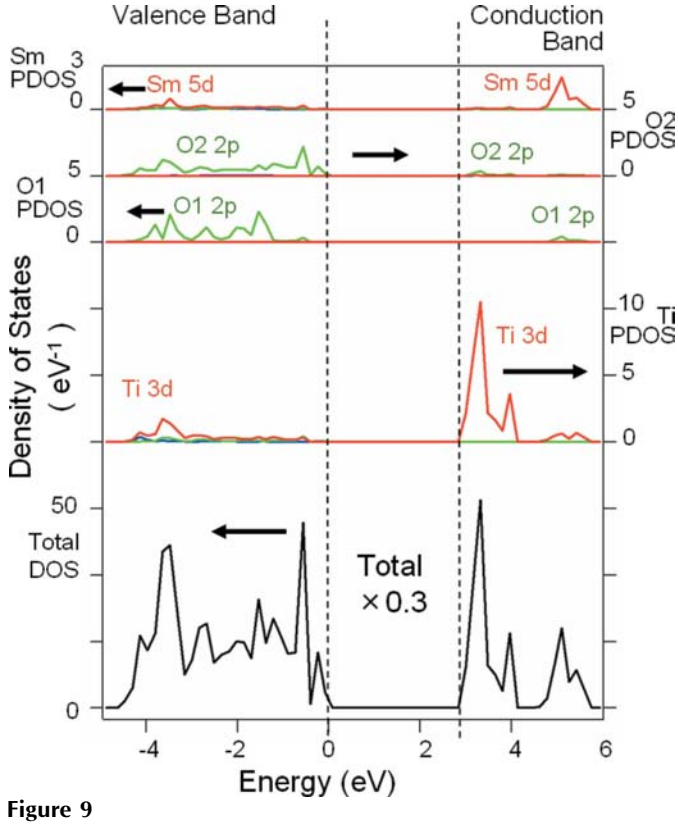

Figure 9
Part of a diagram of total and partial DOS for Ti, O and Sm orbitals in $Sm_2Ti_2O_7$. Blue, green and red lines denote the partial DOS for *s*, *p* and *d* orbitals, respectively. The intensity of the blue lines is negligible. The arrow denotes the scale for the DOS. This figure is in colour in the electronic version of this paper.

8 were prepared using the *VENUS* and *VESTA* programs developed by Dr R. Dilanian, Dr F. Izumi and Mr K. Momma.

References

Blöchl, P. E. (1994). *Phys. Rev. B*, **50**, 17953–17979.
Boyer, C., Deudon, C. & Meerschaut, A. (1999). *C. R. Acad. Sci. Paris Ser. II*, **2**, 93–99.
Brese, N. E. & O'Keeffe, M. (1991). *Acta Cryst.* B**47**, 192–197.
Carp, O., Huisman, C. L. & Reller, A. (2004). *Prog. Solid State Chem.* **32**, 33–177.
Fujishima, A. & Honda, K. (1972). *Nature*, **238**, 37–38.
Fujishima, A., Rao, T. N. & Tryk, D. A. (2000). *J. Photochem. Photobiol. C*, **1**, 1–21.
Goga, M., Seshadri, R., Ksenofontov, V., Guetlich, P. & Tremel, W. (1999). *Chem. Commun.* pp. 979–980.
Hoffmann, M. R., Martin, S. T., Choi, W. & Bahnemann, D. W. (1995). *Chem. Rev.* **95**, 69–96.
Hyett, G., Rutt, O. J., Gal, Z. A., Denis, S. G., Hayward, M. A. & Clarke, S. J. (2004). *J. Am. Chem. Soc.* **126**, 1980–1991.
Ishikawa, A., Takata, T., Kondo, J. N., Hara, M., Kobayashi, H. & Domen, K. (2002). *J. Am. Chem. Soc.* **124**, 13547–13553.
Ishikawa, A., Takata, T., Matsumura, T., Kondo, J. N., Hara, M., Kobayashi, H. & Domen, K. (2004). *J. Phys. Chem. B*, **108**, 2637–2642.
Ishikawa, A., Yamada, Y., Takata, T., Kondo, J. N., Hara, M., Kobayashi, H. & Domen, K. (2003). *Chem. Mater.* **15**, 4442–4446.
Izumi, F. & Dilanian, R. A. (2002). *Recent Res. Dev. Phys.* **3**, 699–726.
Izumi, F. & Ikeda, T. (2000). *Mater. Sci. Forum*, **321–324**, 198–203.
Kresse, G. & Furthmuller, J. (1996). *Phys. Rev. B*, **54**, 11169–11186.
Kresse, G. & Hafner, J. (1993). *Phys. Rev. B*, **47**, R558–R561.
Kresse, G. & Joubert, D. (1999). *Phys. Rev. B*, **59**, 1758–1775.
MacLean, D. A., Ng, H.-N. & Greedan, J. E. (1979). *J. Solid State Chem.* **30**, 35–44.
Mills, A. & Le Hunte, S. (1997). *J. Photochem. Photobiol. A*, **108**, 1–35.
Momma, K. & Izumi, F. (2006). *IUCr Newsl.* **7**, 106–119.
Monkhorst, H. J. & Pack, J. D. (1976). *Phys. Rev. B*, **13**, 5188–5192.
Pechini, M. P. (1967). US Patent, No. 3 330 697.
Perdew, J., Burke, K. & Ernzerhof, M. (1996). *Phys. Rev. Lett.* **77**, 3865–3868.
Toraya, H. (1990). *J. Appl. Cryst.* **23**, 485–491.
Toraya, H., Hibino, H. & Ohsumi, K. (1996). *J. Synchrotron Rad.* **3**, 75–83.
Toraya, H., Huang, T. C. & Wu, Y. (1993). *J. Appl. Cryst.* **26**, 774–777.
Uno, M., Kosuga, A., Okui, M., Horisaka, K. & Yamanaka, S. (2005). *J. Alloy Compd*, **400**, 270–275.
Yashima, M., Ando, Y. & Tabira, Y. (2007). *J. Phys. Chem. B*, **111**, 3609–3613.
Yashima, M., Lee, Y. & Domen, K. (2007). *Chem. Mater.* **19**, 588–593.
Yashima, M. & Tanaka, M. (2004). *J. Appl. Cryst.* **37**, 786–790.
Yashima, M. & Tsunekawa, S. (2006). *Acta Cryst.* B**62**, 161–164.
Yashima, M., Xu, Q., Yoshiasa, A. & Wada, S. (2006). *J. Mater. Chem.* **16**, 4393–4396.